CFD simulation of anti-fogging coatings performance in refrigerated display cabinets

CFD simulation of anti-fogging coatings performance in refrigerated display cabinets

P D'Agaro*, G Croce, N Suzzi

Polytechnic Department of Engineering and Architecture, University of Udine, Italy

* E-mail: paola.dagaro@uniud.it

Abstract. A numerical procedure for the simulation of both fogging and the defogging process on the glass door of a vertical refrigeration display cabinet for chilled food is presented. The large scale problem within the cabinet (convective air flow and heat transfer, moisture mass transport, unsteady conduction through a multi-glazed door) is modelled via a commercial CFD code, whereas the water layer is modelled, via in-house user defined routines, as a collection of tiny droplets in order to take into account the surface wetting properties, the latent heat contributions and the area effective wet fraction. Local water layer equivalent thickness and time needed for the complete defogging are evaluated for different indoor conditions. The influence of anti-fog coatings is investigated comparing different droplets contact angle, from 30° to 90°.

1. Introduction

A cost-effective measure recently applied in commercial refrigeration to achieve energy savings is to employ closed door refrigeration display cabinet not only for frozen food products but even for chilled ones. For retrofitting to current display cabinets, the greatest savings could be achieved by fitting doors on the medium temperature ones [1,2]. A potential drawback is the mist deposition that takes place on the glass surface when the door is opened and condensation of indoor humidity occurs on the cold surface. Once the door is closed, the defogging process should be as fast as possible to re-establish proper visibility of the product through the glass.

In frozen food display cabinets, defogging is usually speeded up by an air curtain flowing along the internal glass surface and by anti-sweat heaters embedded in the door frame or in the glass itself. In chilled display cabinets, the use of anti-fog coatings is more widespread.

The effectiveness of several technological solutions can be profitably assessed by simulation at an early stage of the design process. The fogging/defogging process, in fact, is essentially a conjugate fluid-solid heat and mass transfer problem in presence of a phase changing fluid layer on one side of the solid surface. Furthermore, it is a typical multi-scale problem, where the droplet details (sub-millimeter scale) interact with the cabinet flow structure (meter scale). Some effects, such as the glass surface wettability properties, can be predicted only modelling the water layer as a discontinuous collection of tiny droplets, taking into account the evolution in the droplets size and contact angle.

In the literature, several studies are focused on the characterization of the dropwise condensation of steam on hydrophobic and hydrophilic surfaces. Recently the interest is mostly addressed to the heat transfer enhancement produced by dropwise condensation [3] for new developed surface coatings both via experimental test [4, 5, 6] and via theoretical models [7, 8]. Less references can be found on the dynamics, condensation and evaporation of small scale, low temperature, dew droplets [9, 10].

However, there is a gap between fundamental research on the droplet pattern evolution and its application to the larger scale problems where fogging is detrimental, such as spectacle lens, vehicle windshields, photovoltaic panels, to name a few. The authors aim to contribute in fulfilling this gap by developing a numerical procedure for the simulation of fogging and defogging phenomena which couples the unsteady simulation of the water layer evolution (small scale) to the CFD simulation in the fluid and solid domains adjacent to the surface (large scale). The procedure has been validated in [11] and a simplified version has been applied previously to the prediction of the fogging and defogging processes on a car windshield [12] and on the glass door of refrigerated closed display cabinet for frozen food [13]. Here, a closer integration between the suite of in-house routines for the unsteady simulation of the water layer and a commercial CFD solver is reached and applied to reproduce the physical transient before, during and after the door opening of a refrigerated display cabinet for chilled food. Simulations have been carried out for different indoor conditions and wettability properties of the glass surface.

2. Conjugate fluid/solid problem

The simulation of the fogging/defogging process involves the solution of a conjugate fluid-solid heat and mass transfer problem in presence of a phase changing fluid layer on one side of the solid surface. As stated above, in this specific application the water layer builds up on the cold surface of the multi-glazed door of the cabinet when the glass door is opened and exposed to the free convection of the hot and humid air of the retail store. Defogging takes place when the door is closed and the surface is exposed to the forced convection in the refrigerated volume. A schematic of the physical problem is sketched in figure 1, showing the interface Γ between the solid and fluid domains where the phase change occurs. The unsteady conjugate fluid-solid problem is solved via the finite volume commercial Fluent 17.0 from ANSYS, while the interfacial algorithm modelling the water layer evolution and the latent heat source is implemented via in-house “User Defined Functions” (UDF).

2.1. Solid domain

The glass door is a 4-9-4 mm multi-glazed door, thus the heat transfer process involves conduction in the solid layers and free convection and radiation in the air cavity. An off-line, standalone iterative calculation has been carried out in order to assess the thermal capacity and conductivity of a fictitious solid, which approximates the thermal behavior of the air cavity.

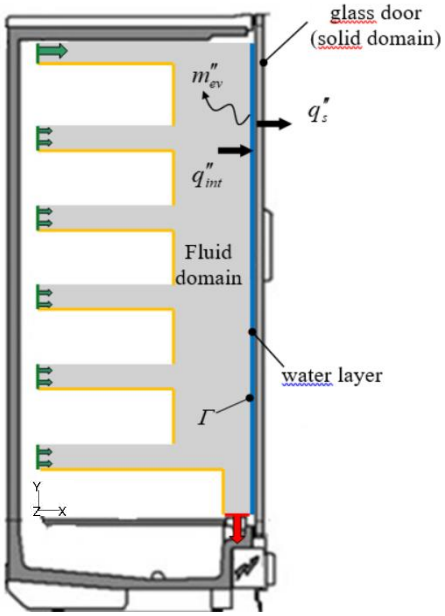

Figure 1. Investigated domain and main boundary conditions.

Thus, only the unsteady conduction problem in the resulting composite wall is solved. A source term is introduced in the energy equation for the inner glass layer in order to include the latent contribution from the condensation/evaporation that takes place on interface Γ. A uniform Robin boundary condition (heat transfer coefficient 8 W/m^{2}K and ambient temperature 26°C, which is the typical indoor design condition for supermarkets in summer) is set at the outer surface.

2.2. Fluid domain

Navier-Stokes, energy and moisture mass transport equations are solved in the fluid domain. Turbulence k-ε model has been adopted. In particular, it is a forced convection problem when the door is closed and a natural convection one when the door is open. The Boussinesq approximation has been assumed for the simulation of natural convection.

2.2.1. Forced convection. Complex forced convection flow fields develop in the refrigerated volume before the door opening (dry condition) and once the door is closed again (evaporation). The mass flow ($1.43\text{x}10^{-3}$ kg/s) of refrigerated air at 2 °C and 90% relative humidity is split between the upper inlet and the perforated back panel and flows downward to the return grill (figure 1). All wall surfaces are set adiabatic, except those representing the chilled food, which are set at constant temperature 4 °C. The domain is geometrically 3D because of the interface routine requirements, but the assumption of symmetry conditions on the lateral sides brings the problem back to the 2D one sketched in figure1. A block structured mesh of 306,880 hexahedral elements, 665 nodes in the vertical *y*-direction, from 41 to 165 nodes in the *x*-direction and 5 in the *z*-direction, has been adopted, with a refinement along the solid surfaces in particular along the interface Γ, where the first node is at 0.64 mm.

A preliminary grid analysis showed that doubling the mesh nodes leads to a variation in computed main global results (such as exit temperature) within 1%.

2.2.2. Natural convection. As long as the door is open, the cold glass surface is exposed to the natural convection of the air in retail store, set to 26 °C temperature and 60% or 65% relative humidity. In order to facilitate the transfer of results between natural and forced convection computations, and to preserve the UDF data structures, the natural convection case domain shares the same topology of the one used for the forced convection. However, the mesh was exponentially stretched in the x-direction to simulate the larger volume of the store: the exponential stretching preserves the mesh resolution close the glass door, while allowing for coarser grid in the far field. The boundary conditions are obviously changed to simulate external free convection on the vertical glass door: upper and lower surfaces adjacent to the door are set to pressure inlet and outlet respectively and an internal adiabatic surface has been added to avoid any effect from the shelves. The boundary condition for the moisture mass transport equation on interface Γ is set to saturation condition and the condensing mass flow rate per unit area is estimated as follows:

$$\dot{m}''_w = \rho_a D\left(\frac{\partial \omega}{\partial n}\right) \tag{1}$$

where ω is the moisture mass fraction, D is the diffusion coefficient of vapour in air.

3. Water layer model and droplet evolution

Under fogging or defogging conditions, the water layer is a collection of tiny droplets. The droplet shape and patterns affect the mass and thermal balance on the water layer and its interaction with the fluid/solid domains. With reference to figure 2, different surfaces may be identified: A_{wet} and A_{dry} are the areas of the wet and dry portions of the solid interface Γ respectively; A_{cap} is the area of the droplet/fluid interface, which is assumed as a spherical cap and depends on the contact angle ϑ [10]. Neglecting the thermal capacity and thermal resistance of the water layer, due to the small droplet size, the instantaneous thermal balance at each control volume of interface Γ yields:

$$q_s'' = q_{\text{int}}'' \frac{A_{wet} + A_{dry}}{A_t} + \dot{m}_w'' \frac{A_{cap}}{A_t} \lambda\left(T_\Gamma\right) = q_{\text{int}}'' + \dot{m}_w'' \frac{A_{cap}}{A_t} \lambda\left(T_\Gamma\right) \tag{2}$$

where $A_t = A_{wet} + A_{dry}$ is the face area at the interface Γ, q_s'' the conduction heat flux per unit area from the solid, q_{int}'' is the convective flux per unit area to the air, $\dot{m}_w''$ is the evaporating ($\dot{m}_w'' > 0$) or condensing ($\dot{m}_w'' < 0$) mass flow rate from equation (1), λ is the evaporation latent heat at the local interface temperature T_Γ from the solution of the conjugate fluid/solid problem. The latent contribution $\dot{m}_w''\left(A_{cap}/A_t\right)\lambda\left(T_\Gamma\right)$ from the water layer is entered as source term (condensation) or heat sink (evaporation) in the energy equation at the inner glass layer of the door. The surface tension at the droplets' edge and adhesion at the droplets bases are strong enough to prevent shear or gravity driven water flow along the surface; thus, the transient mass balance can be simplified as follows:

$$\rho_w \frac{\partial H}{\partial t} = -\frac{A_{cap}}{A_t} \dot{m}_w'' \tag{3}$$

where H is the cell-averaged local water layer height. The droplet evolution during condensing and evaporating process affects the area ratios in equations (2) and equation (3). The model for the droplet evolution is described in detail in [11]. Here, we recall that the condensation process leads to self-similarity regime in the droplet pattern [9]: throughout the condensation process the contact angle ϑ remains constant and the surface coverage is approximately 55% of the total area of the solid surface A_t [11]. This allows for an estimate of the A_{cap}/A_t ratio for any given contact angle. In the evaporation process two different stages may be distinguished: a first stage during which the base area of the droplet is constant while the contact angle decreases to the receding value (see figure 3, t = 1, 2, 3, 4); a second stage the contact angle is preserved and the droplet volume reduction yields a wet area decrease (see figure 3, t = 5, 6). The above described phenomena is modelled as reported in [11], allowing the evaluation of the area ratios in equation (2).

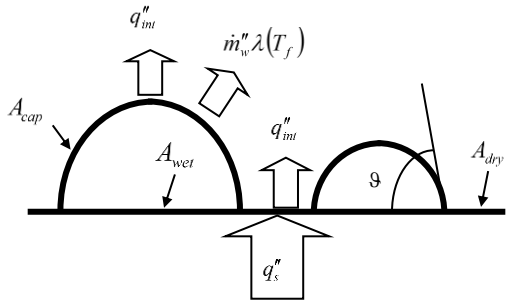

Figure 2. Water layer: surfaces, contact angle ϑ, heat fluxes.

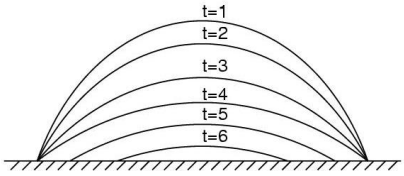

Figure 3. Droplet shape evolution during evaporation.

4. Results and discussion

The simulation at dry conditions (without water layer at the interface) is carried out to solve the steady state solution for the velocity, temperature and moisture fields in the refrigerated volume as well as the temperature distribution in the glass door just before the door opening.

In figure 4, streamlines colored with the velocity variable show the resulting flow structure. The air flows from the main top inlet to the return grill: the high velocities through the main inlet, however,

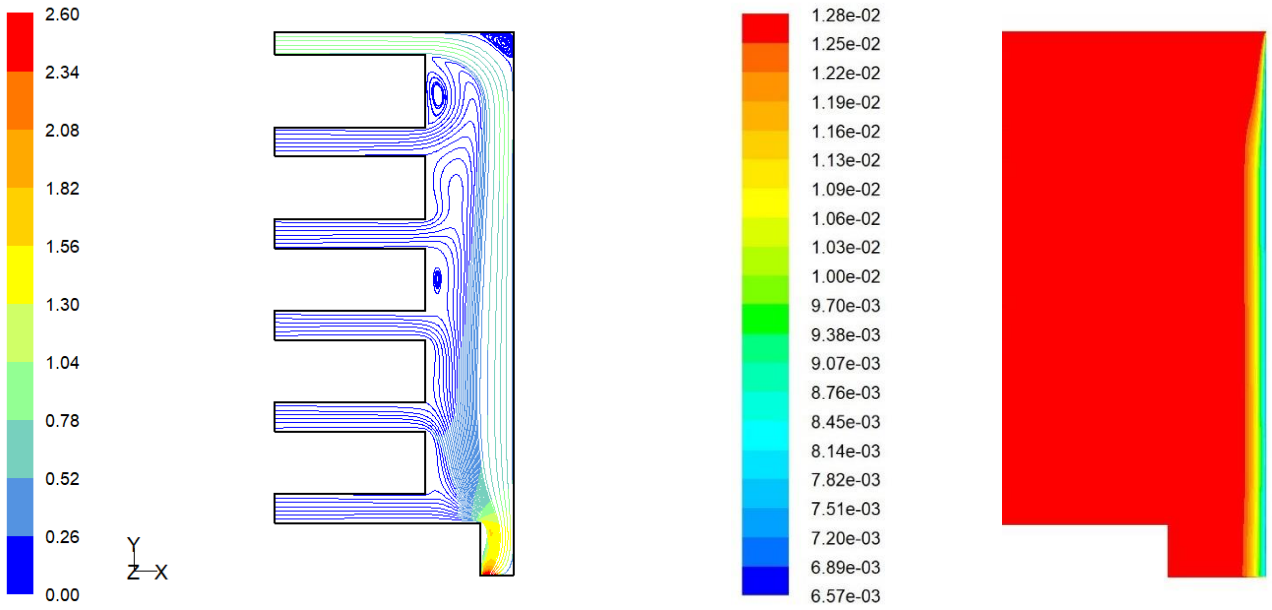

Figure 4. Left: streamlines colored with velocity variable (dry simulation, closed cabinet). Right: ω distribution after 30 s of the condensation process (relative humidity ϕ=60%, open door).

produce a recirculation on the face of the top load, and an entrainment effect that partially deviates upward the mass flow entering from the two upper perforated plates. This effect vanishes in the lower part of the cabinet, and the streamlines coming from the three lower perforated back plates simply flows down following the main curtain. A smaller fluid recirculation appears close to the top of glass, as well.

The moisture concentration field (figure 4b) shows the development of the glass door boundary layer in the condensation process. The apparent change in the slope of the layer growth in the upper area of the door is related to the local temperature peaks, as will appear from the following pictures.

Transient simulations of the condensation process are carried out with a 0.5 s time step up to 30 s door opening time for two values of the indoor relative humidity (ϕ=60% and ϕ=65%) and two values of droplets contact angle: ϑ = 90°, representative of a slightly dirty glass surface, and ϑ = 30° representative of hydrophilic anti-fog coating.

In figure 5 the temperature distribution along the glass surface Γ is shown at the beginning (0 s) and at the end of the condensation process (30s); it presents a global minimum value at the impinging of the main air curtain and a local one where the flow is accelerated at the return grill (see streamlines in figure 4). The 30 seconds exposition to warm indoor air at 26 °C causes a temperature increase from 1.5 to 2.4 K along the surface.

The water layer at the end of 30 s door opening is reported in figure 5 in terms of equivalent thickness H defined in equation (3).The water layer is very thin, but the effect of the different surface wettability is substantial: the contact angle ϑ = 30° reduces the condensate deposition approximatively by half with respect to the bare glass (ϑ = 90°). The influence of the relative humidity is appreciable as well; the water layer is around 22% thicker in the central zone (at y = 0.8 m) for ϕ = 65% with respect to ϕ = 60%.

The transient simulation of the defogging process is carried out with a 0.5 s time step; the initial condition in the fluid domain for each case is the steady state solution of the dry simulation; the temperature field and water layer characteristics at the end of the condensation process are the initial conditions in the solid domain. The evolution of the water layer thickness is reported in figure 6 at 2.5 seconds intervals for the case study ϕ=65% and ϑ = 90°. The evaporation process slows down with time, the water layer thickness is reduced by half in the central zone (y=0.8) in approximatively 7.5 s but and it requires 12.5 s more to dry completely. It can be noticed that a very small area at the top and

at the bottom, where the fluid recirculations are detected, isn't completely dry neither after 20 s from the beginning at the evaporation process.

The comparison among the water layer distributions after 12.5 s from the beginning of the defogging process is depicted in figure 7. It shows that the glass with anti-fog coating (ϑ = 30°) is almost completely dry for indoor relative humidity ϕ=60%, except for the already mentioned very small area at the top and bottom. At ϕ=65% a very thin layer is still present in the central area and it requires 2.5 s more to dry completely.

On the contrary, the bare glass (ϑ = 90°) is still almost completely wet at 12.5 s both for indoor relative humidity ϕ=65% (wet surface fraction equal to 95%) and for ϕ=60% (wet surface fraction equal to 81%). Complete defogging requires almost 5 s more than the anti-fog solution at the same indoor conditions.

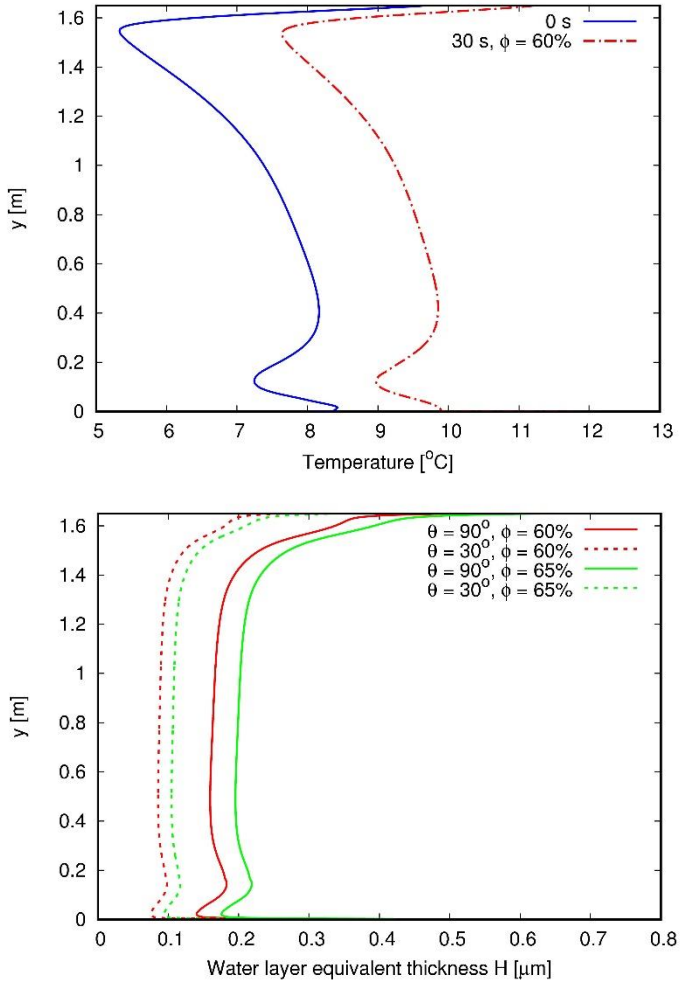

Figure 5. Condensation process: temperature (top) and water layer equivalent thickness (bottom) distributions along interface Γ at the beginning (0 s) and at the end (30s) of the door opening time.

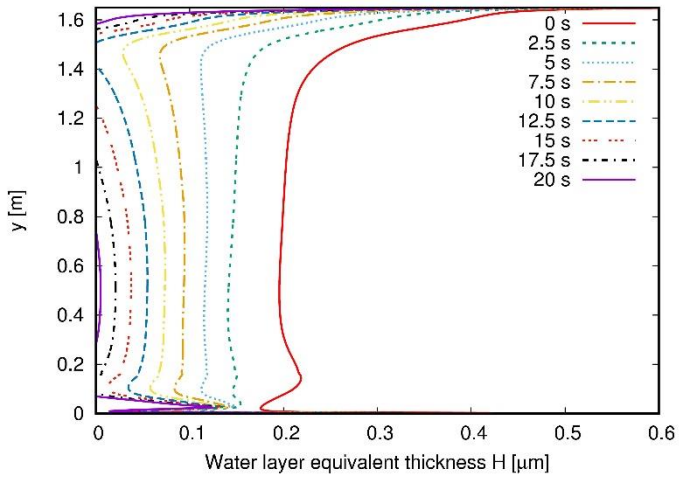

Figure 6. Evaporation process: water layer evolution along the interface Γ for ϕ=65% and ϑ = 90°.

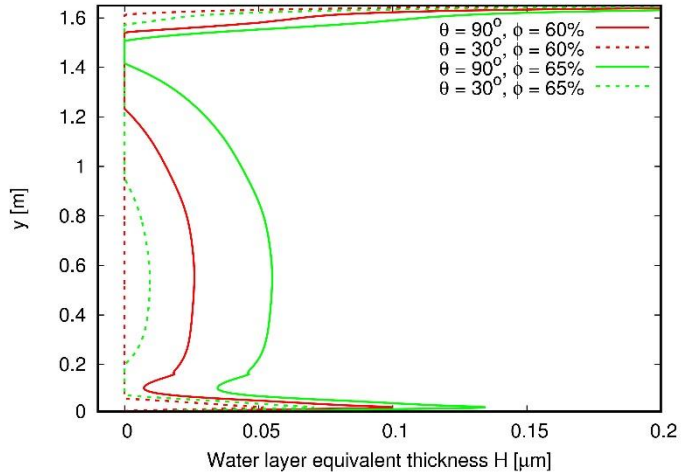

Figure 7. Comparison of the water layer thickness after 12.5 s from the beginning of the defogging process.

5. Conclusions

A numerical procedure has been applied for the simulation of both fogging and the defogging process on the glass door of a vertical refrigeration display cabinet for chilled food. Modeling the water layer as a collection of tiny droplets allows to take into account the effect of the surface wetting properties on the condensate deposition process and on the resulting time needed for the complete defogging.

The use of an anti-fog coating, decreasing the droplet contact angle from 90° to 30°, yields a 50% reduction of the condensate deposition. In the solution with anti-fog coating, the time needed for the complete defogging, after a door opening time of 30s, is around 30 % lower than that needed by the bare glass. Thus, it is an effective solution to reduce or to avoid the fogging phenomena for chilled food display cabinet and to keep the defogging time within reasonable values at the most common humidity conditions in retail stores.

References

[1] Carbon Trust 2010 Refrigeration Road Map – An Action Plan for the Retail Sector (CTG021).

[2] Foster A, Hammond E, Brown T, Maidment and G, Evans J 2018. Technological Options for Retail Refrigeration; International Institute of Refrigeration pp 33-38.
[3] J.W. Rose J W 2002 *J. Power Energy* **216** 115–128.
[4] Parin R, Bortolin S, Martucci A, Del Col D 2018 *Proc.16th International Heat Transfer Conference* (Beijing) pp 2307-14.
[5] Parin R, Tancon M, Mirafiori M, Bortolin S, Moro L, Zago L, Carraro F, Martucci A, Del Col D 2020 *Applied Thermal Eng.* **179** 115718.
[6] Vemuri S, Kim K J, Wood B D, Govindaraju S, Bell T W, 2006 *Applied Thermal Eng* **26** 421–429.
[7] Kim S, Kim K J 2011 *J. Heat Transfer* **133** 081502
[8] Croce G, D'Agaro P, Suzzi N, 2019 *Proc. ICNMM2019* (St. John's, NL, Canada) Paper No: 4291.
[9] Beysens D 1995 *Atmospheric Research* **39** 215-237.
[10] Chandra S, di Marzo M, Qiao Y M and Tartarini P 1996 *Fire Safety J.* **27** 141–158.
[11] Croce G, D'Agaro P and Della Mora F 2005 *Int. J. Computational Fluid Dynamics* **19** 437–445.
[12] Croce G, D'Agaro P, De Angelis A and Mattiello F 2007 *IMechE Part D: Journal of Automobile Eng.* **221** 1241-50.
[13] D'Agaro P, Croce G. and Cortella G 2006 *Applied Thermal Eng.* **26** 1927-34.